ALTIGLACIO - Marché sous accord-cadre n°180579

Lot 1-task 1.2: multi-mission sea level in the Arctic Ocean

Reference:	CLS-ENV-NT-20-0126
Nomenclature:	-
Issue:	1. 1
Date:	2020,Apr.03

CLS headquarters
11 rue Hermès
Parc technologique du Canal
31520 Ramonville Saint-Agne
FRANCE

Tel. +33 (0)5 61 39 47 00
Fax +33 (0)5 61 75 10 14
Mail: info@cls.fr
www.cls.fr

CLS Brest Le Ponant
Zone du technopôle de Brest Iroise
Avenue La Pérouse
29280 Plouzané
FRANCE

Tel. 33 (0)2.98.05.76.80
Fax 33 (0)2.98.05.76.90

Chronology Issues:

Issue:	Date:	Reason for change:	Author
1.0	10/03/20	Creation	P. Prandi
1.1	03/04/20	Revisions following CNES remarks	P. Prandi

People involved in this issue:

Written by (*):	P. Prandi	Date + Initials:(visa or ref)
Checked by (*):	NA	Date + Initial:(visa ou ref) [Checker]
Approved by (*):	NA	Date + Initial:(visa ou ref) [Approver]
Application authorized by (*):	NA	Date + Initial:(visa ou ref)

In the opposite box: Last and First name of the person + company if different from CLS

Index Sheet:

Context:	
Keywords:	[Mots clés]
Hyperlink:	

Distribution:

Company	Means of distribution	Names
CLS	Notification	P. Prandi, P. Thibaut, Y. Faugère, J-C. Poisson
CNES	Notification	A. Guillot.

FORM-NT-GB-10-1

List of tables and figures

List of tables:

Aucune entrée de table d'illustration n'a été trouvée.

List of figures:

List of items to be confirmed or to be defined

Lists of TBC:

Aucune entrée de table des matières n'a été trouvée.

Lists of TBD:

Aucune entrée de table des matières n'a été trouvée.

Applicable documents

AD 1 Plan d'assurance produit de CLS
CLS-ED-NT-03-394

Reference documents

RD 1 Manuel du processus Documentation
CLS-DOC

RD 2 Armitage, T. W. K., Bacon, S., Ridout, A. L., Thomas, S. F., Aksenov, Y., and Wingham, D. J. (2016), Arctic sea surface height variability and change from satellite radar altimetry and GRACE, 2003–2014, J. Geophys. Res. Oceans, 121, 4303– 4322, doi:10.1002/2015JC011579

RD 3 Proshutinsky, A. Y., and Johnson, M. A. (1997), Two circulation regimes of the wind-driven Arctic Ocean, J. Geophys. Res., 102(C6), 12493– 12514, doi:10.1029/97JC00738.

RD 4 Stine Kildegaard Rose, Ole Baltazar Andersen, Marcello Passaro, Carsten Ankjær Ludwigsen andChristian Schwatke, Arctic Ocean Sea Level Record from the Complete Radar Altimetry Era: 1991–2018, Remote Sens. 2019, 11(14), 1672; https://doi.org/10.3390/rs11141672

RD 5 Peacock, N. R. and Laxon, S., Sea surface height determination in the Arctic Ocean from ERS altimetry, JGR-Oceans, 2004, 109

RD 6 Poisson, J.C.; Quartly, G.D.; Kurekin, A.A.; Thibaut, P.; Hoang, D.; Nencioli, F. Development of an ENVISAT altimetry processor providing sea level continuity between open ocean and Arctic leads. IEEE Trans. Geosci. Remote Sens. 2018, 56, 5299–5319.

RD 7 Prandi, P., Mono-mission sea level in the Arctic Ocean, CLS-ENV-NT-19-0341

FORM-NT-GB-10-1

List of Contents

1. Introduction

The present document summarizes the studies performed in the frame of the CNES AltiDoppler glaciologie 2018 contract (n°180579), lot 1, task 1.2 to combine sea surface measurements in the Arctic Ocean.
Here we address multi-mission combination only, mono-mission analysis are detailed in a previous report (RD 7).
All currently available sea surface topography datasets in the Arctic Ocean rely on only one mission at a time: no multi-mission combination is performed, either in dynamic topography fields of Armitage et al., 2016 (RD2) or sea level anomalies by Rose et al., 2019 (RD 4).

Here we rely on mono-mission sea level anomalies in the Arctic Ocean generated earlier in the frame of the CNES AltiDoppler glaciologie project to prototype a multi-mission analysis of the Arctic Ocean. This analysis aims at leveraging a three missions constellation (SARAL/AltiKa, Sentinel-3A and CryoSat-2) to improve the resolution of sea level anomaly fields in the Arctic Ocean both in time and space.

In this document we describe the data processing scheme used to generate sea level anomaly maps for the Arctic Ocean from the combination of along-track radar altimeter measurements and some validation results.

2. Data processing overview

For this analysis, our starting point are along-track sea level anomaly measurements that where generated as part as Task 1.1 of the project. Sea level anomaly estimation from raw altimeter measurements is detailed in a specific report (DR 7). The focus here is on generating Level 4 products from Level 2 outputs. Processing steps are represented on the scheme of Figure 1.
First a basic cross-calibration based on the mono-mission products is applied to reference Sentinel-3A and CrysoSat-2 to SARAL/AltiKa because SARAL/AltiKa data are based on the Adaptive retracker ensuring continuity between open and ice-covered ocean. Along-track measurements are then extracted separately for the open ocean and ice-covered areas for each mission. The open ocean measurements are filtered and subsampled to construct a 5 Hz along-track product. Measurements from leads are left as is. The optimal interpolation relies on the current DUACS methodology and produces SLA maps combining all three missions together.

We processed the period where three missions are available, which is limited by the availability of Sentinel-3A. The final product covers almost two years from July 2016 to June 2018. The SLA field is estimated every three days on a 25km resolution grid.

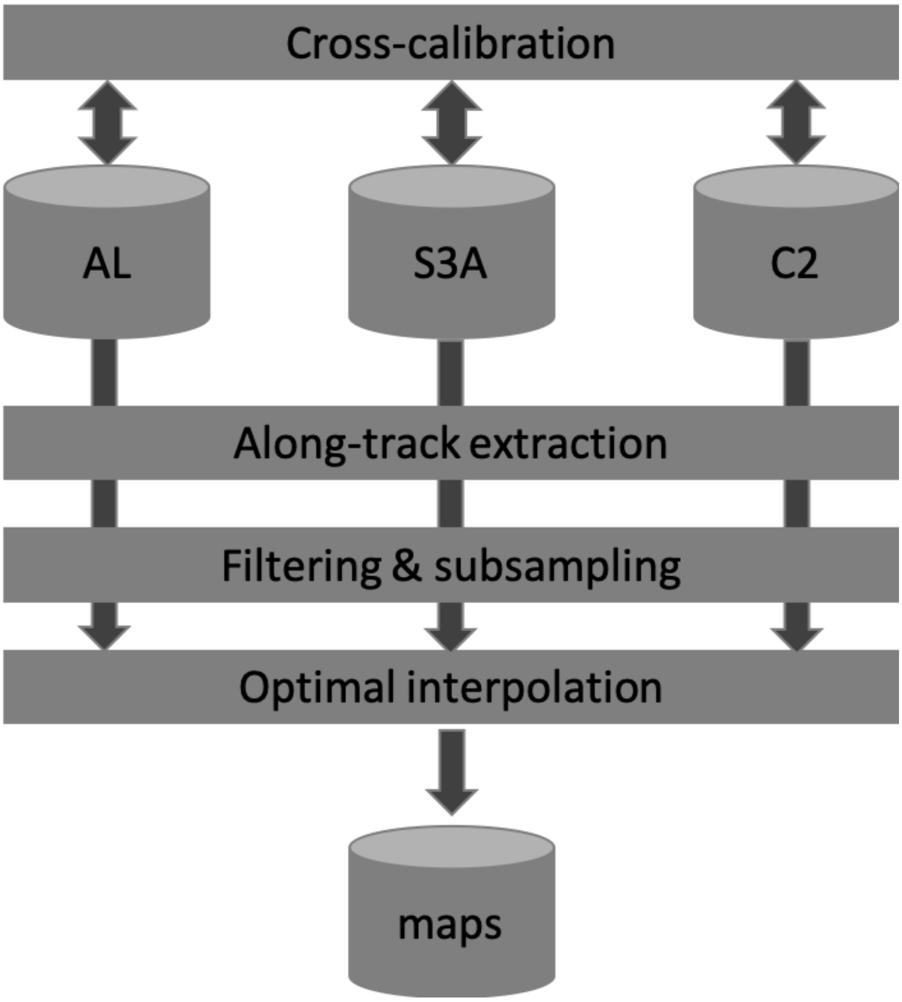

Figure 1, data processing overview

3. Cross-calibration

The cross-calibration is designed to remove large scale biases between different missions. For DUACS global processing the empirical orbit error typically removes signals at one and two cycles per revolution based on SSH differences at crossovers. The same approach is impossible here as it would require to compute crossovers globally. Moreover empirical orbit errors are likely inaccurate in the Arctic Ocean, a basin surrounded by large continents, where no cross-overs are available to constrain the solution.
We already showed that mono-mission datasets are in good agreement in the Arctic Ocean, as demonstrated on **Figure** 2 (copied from DR 7). To perform a more detailed analysis we estimated time series of SLA differences over the Arctic Ocean for Sentinel-3A minus SARAL/AltiKa and CryoSat-2 minus SARAL/AltiKa, for non-overlapping 10 day windows. In both cases the differences exhibit a clear annual cycle of centimetre-level amplitude (Figure 3).
In order to correct for this signal, we fit and remove a sine wave with yearly period.

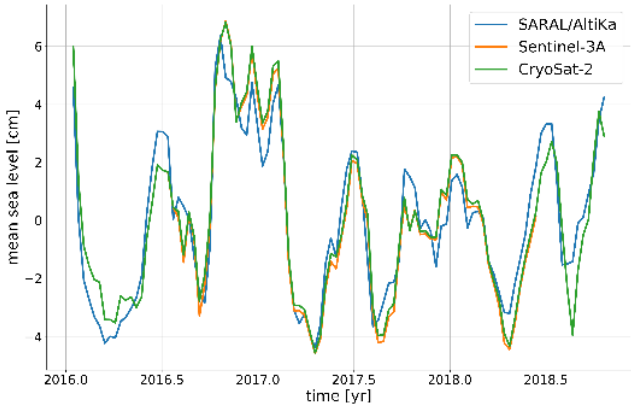

Figure 2, Arctic regional sea level time series from SARAL/AltiKa, Sentinel-3A and CryoSat-2

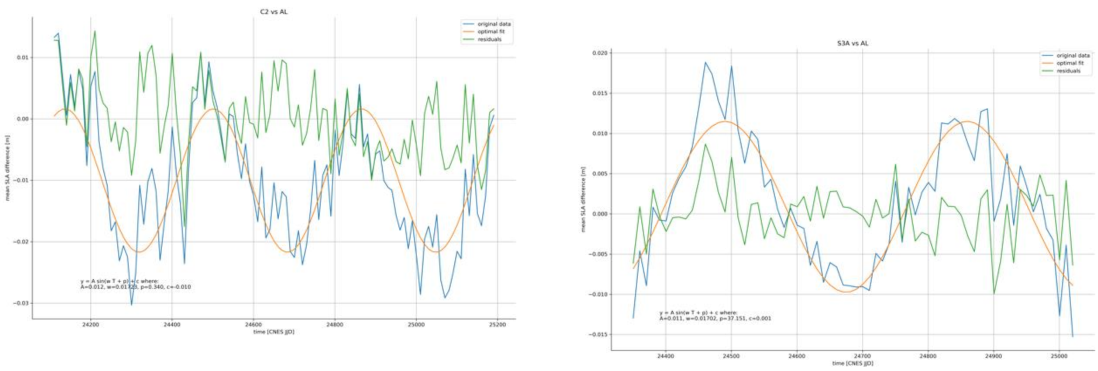

Figure 3, time series of mean SLA differences for CryoSat-2 minus SARAL (left) and Sentinel-3A minus SARAL (right). The non cross-calibrated differences are in blue the yearly fit in orange and the calibrated data in green

After this time-dependent correction is applied to Sentinel-3A and CryoSat-2 data we check the SLA differences for any geographical pattern (Figure 4). Clearly this very simple cross-calibration leaves some level of geographically correlated differences between the missions. Differences are large in the Canadian Arctic Archipelago, and at the sea-ice edge for CryoSat-2 and generally much smaller inside the Arctic Ocean. The CryoSat-2 minus SARAL/AltiKa map has no values over open ocean because we only process CryoSat-2 SAR mode measurements, which is only activated over sea-ice.

Implementing a better cross-calibration method would certainly be beneficial to the quality of the final product (for example fitting a bias on two consecutive tracks, based on regional crossover differences).

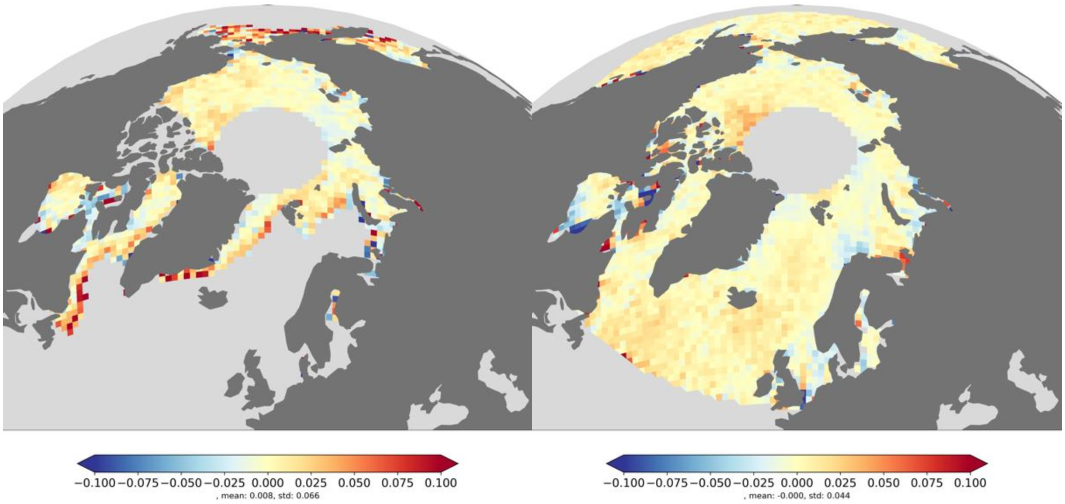

Figure 4, mean bias between CryoSat-2 and SARAL (left) and Sentinel-3A and SARAL (right), in meters.

4. Along-track filtering and subsampling

Before the optimal interpolation, SSH measurements are converted from the internal database format to an along-track netCDF format called residuals. Open ocean and ice covered areas are converted in different files. This allows to filter and sub-sample open ocean measurements. An example of the along-track impact of this filtering and sub-sampling is shown below (Figure 5), for one section of a Sentinel-3A track. The goal of this step is to have an equivalent 5Hz product over open ocean. Investigations over the Southern Ocean showed that using the full 40Hz/20Hz resolution, combined with a 1000 observations limit during the optimal interpolation lead to restricting the area influence around each estimation position to very small volume, which is unwanted.
Measurements from leads are left untouched, at the full resolution of the altimeter. In the long-term perspective of providing along-track SSH measurements, for example for data assimilation, the issue of filtering and/or subsampling these measurements (characterized by large along-track gaps) will have to be addressed.

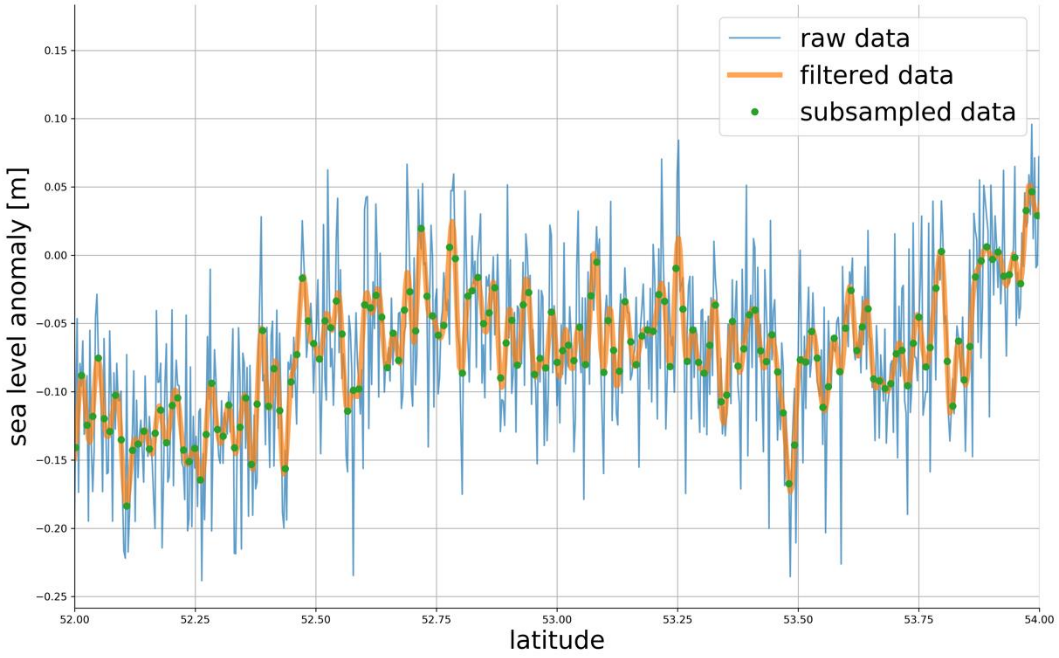

Figure 5, raw, filtered and subsampled sea level anomalies along an open-ocean section of a Sentinel-3A track

5. Optimal interpolation

The optimal interpolation scheme used here is the one that is currently used by DUACS. Only minor modifications are made:

- Interpolation positions follow the EASE2 grid, not a conventional lat/lon regular grid,
- Auxiliary files are updated to reflect the dynamics of the Arctic Ocean as much as possible.

The update of these auxiliary files is described below.

5.1. Signal variance

An accurate a priori signal variance is essential for the quality of the interpolated fields. This value is defined in a gridded NetCDF file, and interpolated at each position of interpolation. A map of file currently used by the DUACS processing is given on Figure 6 and shows that variance levels drop inside the Arctic Ocean. An analysis of variance levels derived from CPOM and DTU Arctic datasets shows that variance levels do not drop that much inside the Arctic Ocean (Figure 7).
For this analysis, we combine those three sources of information by maxing out the signal variance, the resulting signal variance file used is shown on Figure 8.
This is clearly a first guess at signal variance, and should be updated in an iterative way for the next generation of product. By maxing out variance from available sources, we tried to prevent the interpolation from damping observed signals too much.

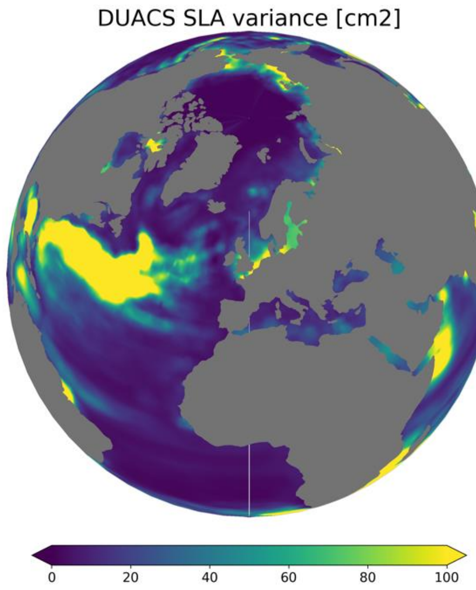

Figure 6, SLA variance used for DUACS global processing.

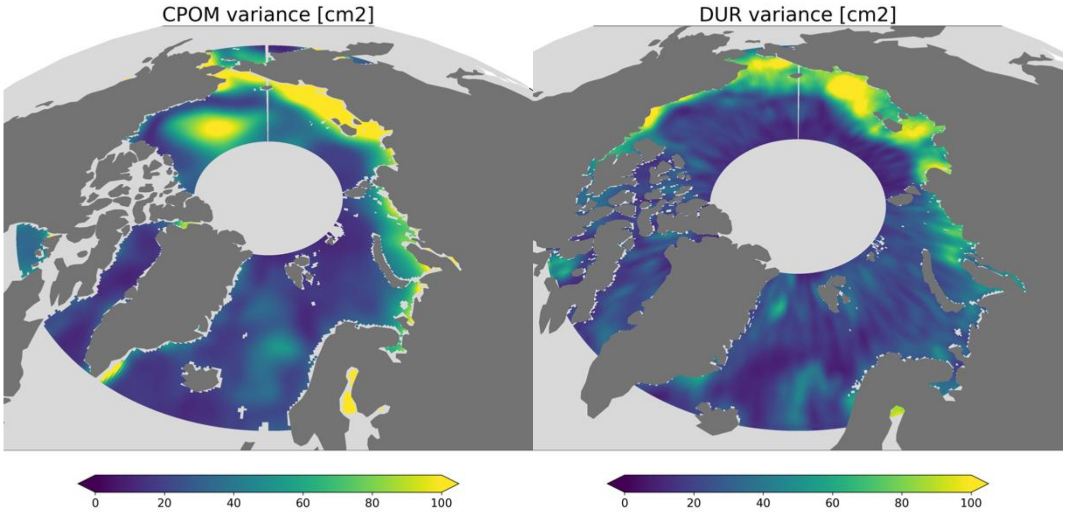

Figure 7, SLA variance levels from the CPOM (left) and DTU (right) datasets.

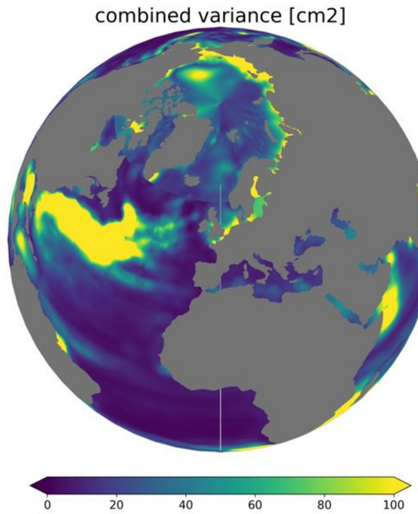

Figure 8, SLA variance used in the objective analysis.

5.2. Noise levels

Another important aspects are noise levels. Accurate noise levels will prevent measurement noise to be interpreted as real signals during the interpolation. DUACS standard processing uses different noise levels for each mission, reflecting the actual level of noise of each mission, plus the unobservable part of the ocean dynamics. These noise levels are shown for SARAL/AltiKa, CryoSat-2 and Sentinel-3A on Figure 9. While SARAL and Sentinel-3 show very low noise levels in the Arctic Ocean, which are unrealistically optimistic, CryoSat-2 defaults to a very high noise level in the Arctic Ocean, especially above 82°North. While this is not a problem for DUACS, as these areas are not mapped due to sea-ice cover, this is not something we want to convey in our analysis.

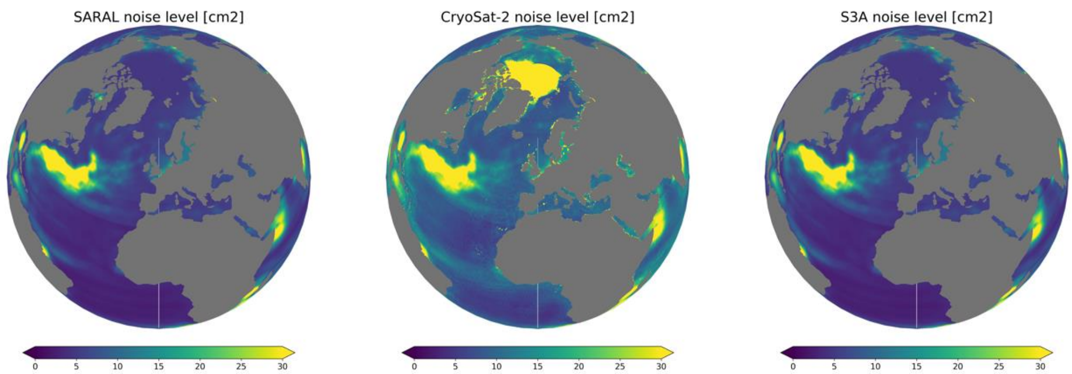

Figure 9, noise levels from DUACS for SARAL/AltiKa, CryoSat-2 and Sentinel-3A

Here we construct to different noise level files, based on the existing DUACS noise levels, depending on whether measurements are over open ocean or over sea-ice. The assumptions used build these estimates are:

- Over ocean, our measurements should slightly noisier than current missions: we are using a model wet tropospheric correction and a less accurate mean sea surface model,
- Over sea-ice, noise level should be even higher due to increased errors in geophysical corrections and in range retrieval from peaky waveforms.
- Noise levels should be scaled to account for the fact that we are using 5Hz or 20(40)Hz measurements depending on the surface.

For the open ocean, the noise level is derived from the SARAL/AltiKa file (to avoid unrealistic values inside the basin) augmented to match CryoSat-2 noise levels in open ocean. Sea-ice noise level is obtained from a similar methodology, but adding 5 cm^2 everywhere. Results are shown on Figure 10. In our analysis, all missions use the same noise levels.

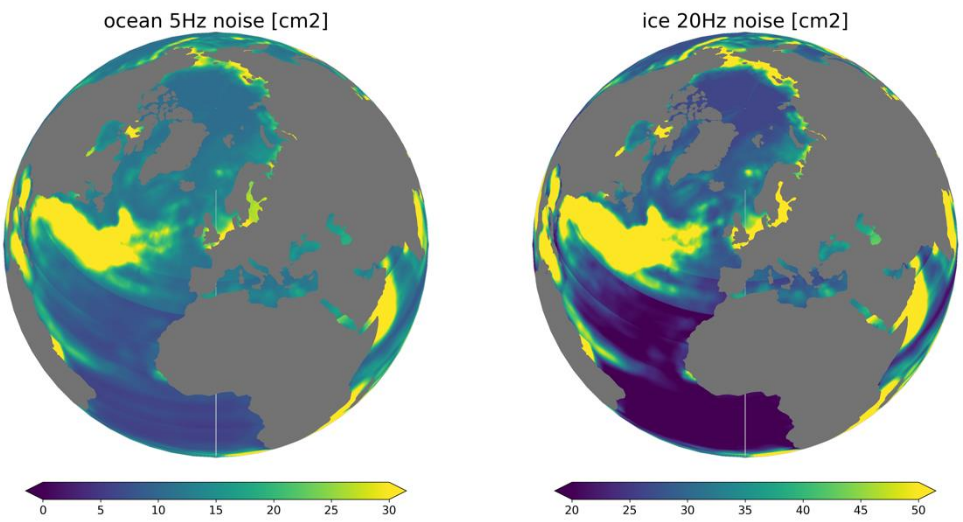

Figure 10, open ocean and leads noise levels used in this analyis, colorbars are different in both plots.

5.3. Long wavelength errors

Long wavelength errors (LWE) are designed to remove correlated errors along-track, coming from errors in geophysical models such as the tide and DAC corrections. In the mapping process, these are considered as an error. Again we derive the LWE used here from existing DUACS files, which are shown on figure Figure 11. There are large differences between the three missions. For example, Sentinel-3A has no LWE variance at high latitudes. For the current analysis, we start from CryoSat-2 LWE error, which exhibits the most variance at high latitudes and set a minimum LWE variance of 10 cm2 for all latitudes greater than 68°N. The resulting LWE variance distribution, which is used for all three missions considered here is shown on Figure 12.

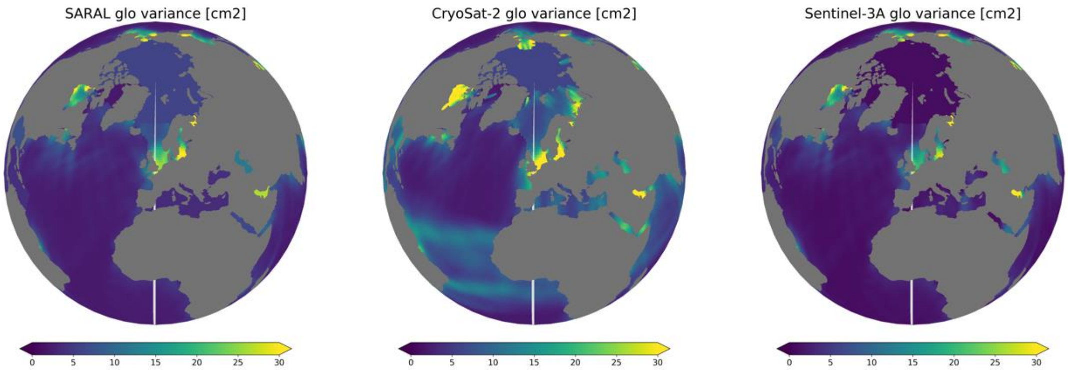

Figure 11, LWE error variance from DUACS

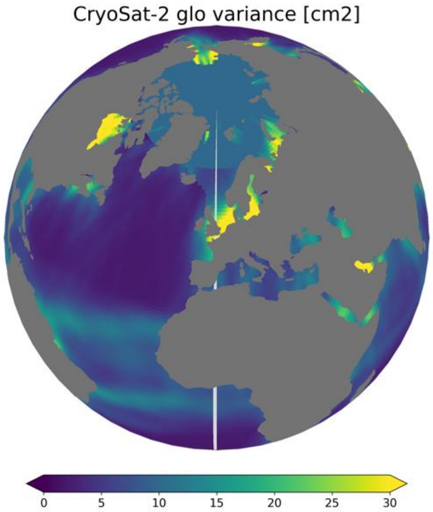

Figure 12, map of the LWE variance used in this analyis

5.4. Correlation scales

Correlation scales are kept unchanged from the standard DUACS processing, and are shown in the time, meridional and zonal directions on Figure 13. While patterns are unphysical, we know that structures in the Arctic Ocean are small. Re-estimation of correlation scales from the CPOM dataset for example would have led to much larger scales while we try to target smaller structures.
Future improvements would be to re-estimate these correlation scales, either from the altimetric measurements used in this study or from an ocean circulation model for example.

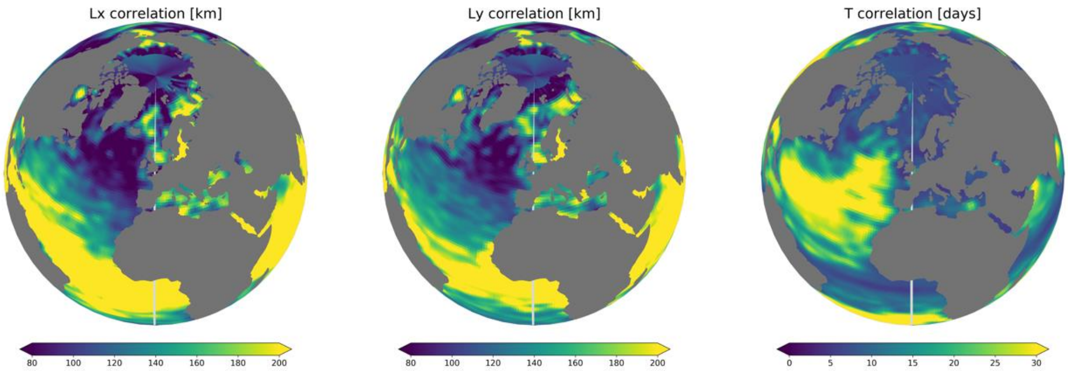

Figure 13, correlation scales used for the optimal interpolation

6. Product format

The multi-mission sea level anomalies are distributed through a netCDF file. The format of the this file is described below.

```
netcdf msla_25km {
dimensions:
        time = 244 ;
        x = 720 ;
        y = 720 ;
variables:
        double sla(time, x, y) ;
                sla:_FillValue = NaN ;
                sla:units = "m" ;
                sla:coordinates = "longitude latitude" ;
        double error(time, x, y) ;
                error:_FillValue = NaN ;
                error:units = "cm" ;
                error:coordinates = "longitude latitude" ;
        double error_percent(time, x, y) ;
                error_percent:_FillValue = NaN ;
                error_percent:units = "percent" ;
                error_percent:coordinates = "longitude latitude" ;
        double date_jjd(time) ;
                date_jjd:_FillValue = NaN ;
                date_jjd:units = "days since 1950-01-01" ;
        double longitude(x, y) ;
                longitude:_FillValue = NaN ;
        double latitude(x, y) ;
                latitude:_FillValue = NaN ;
        int64 time(time) ;
                time:units = "days since 2016-07-01 00:00:00" ;
                time:calendar = "proleptic_gregorian" ;
}
```

Longitudes and latitudes define the actual position of estimation. The date of each grid is expressed in two different variables, as CNES decimal julian days (date_jjd) and as a standard numpy datetimes for ease of use.
The sla variable holds the sea level anomaly field, while the error and error_percent hold formal error estimations either in cm or relative to the signal variance.

FORM-NT-GB-7-1

The SLA field is estimated on a 25km resolution grid, for all latitudes greater than 50°N, every three days, resulting in 244 time steps.

7. Validation results

As for the mono-mission product, validation results presented here are mainly qualitative.

7.1. Geographical distribution

The geographical distribution of the mean and variance of SLA over the whole period is shown on Figure 14. They are generally consistent with findings based on mono-mission analysis: there is a doming in the Beaufort Gyre area, high variance levels are mainly trapped at the coast. However several new features are visible:

- A low SLA bias in the SARIn patch of CryoSat-2, which was not visible in the CryoSat-2 mono-mission analysis, likely due the poorer resolution achievable is now obviously present. It is unclear who is to blame for this as there is no SARIn mode activated over this region over the period considered here. This may be an error in the mean sea surface used (DTU15).
- Some track shaped patterns are visible, mainly off the coast of Russia, indicating that improvements of the cross-calibration method might be needed. Another possible source is that the auxiliary files (see Figure 8 for example) result in these king of patterns. We will conduct an experiment using constant values for all auxiliary files to investigate this.
- Variance levels drop above 82°N where only CryoSat-2 measurements are available.

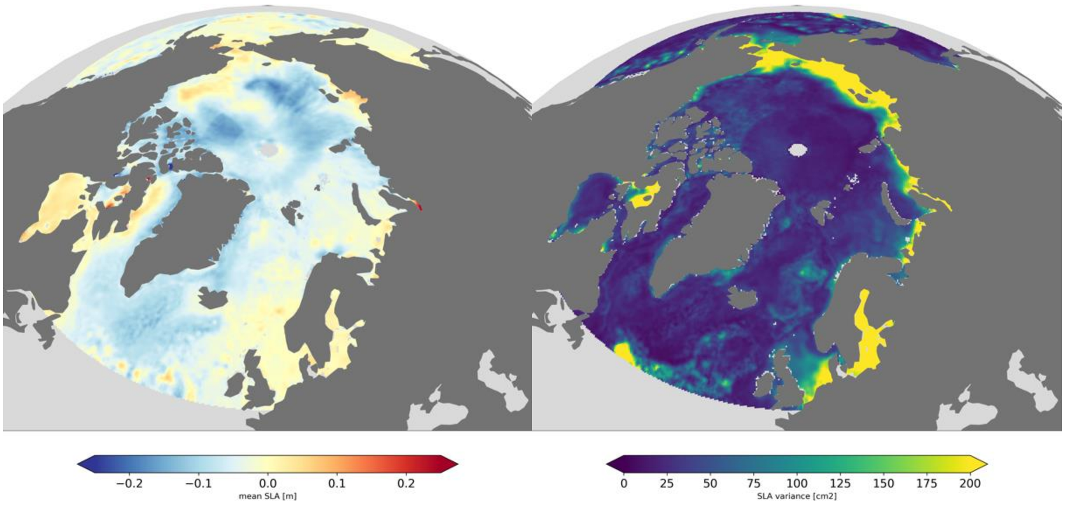

Figure 14, mean (left) and variance (right) of SLA fields from the multi-mission product

7.2. Temporal evolution

The temporal evolution of the regional Arctic Ocean sea level is provided as Figure 15. The main feature is a yearly signal, which is expected. This yearly signal reaches minimum in winter, where sea-ice extent is maximum, which does not support freeboard contamination in sea level estimation.
Attempts to relate the temporal evolution of the regional mean sea level (or its principal components) to the Arctic Oscillation Index remained unsuccessful.

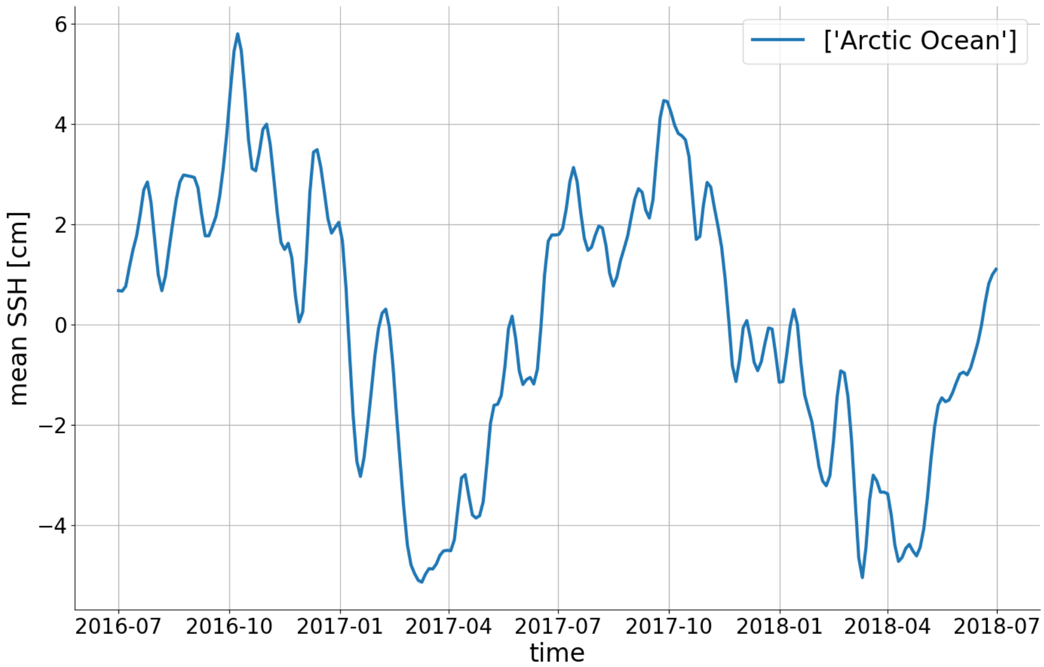

Figure 15, mean Arctic sea level derived from the multi-mission grids, in cm

7.3. Comparisons to DUACS global product

The product generated within the frame of this project focuses on the Arctic Ocean and we know its accuracy over open ocean is hindered by some processing choices such as using the modelled wet tropospheric correction, or not estimating empirical orbit error corrections. Comparing the Arctic Ocean product with DUACS global dataset is a way to assess that despite these processing choices, we still have an acceptable performance over open ocean surfaces.
To perform this comparison, DUACS grids are bilinearly interpolated onto the 25 km EASE2 grid used for the Arctic Ocean product.
The mean and variance of SSH differences are shown on Figure 16. Largest differences are found in the interior of the Arctic Ocean, as expected. It this area, the DUACS global product is largely inaccurate (all measurements affected by sea-ice are removed by the editing). In the open ocean the variance of differences is generally low, but some biases between products appear. These are likely related to differing standards. The strong gradient in the Atlantic Ocean, between Iceland

and Norway is likely related to the different mean sea surfaces used in both products (DTU15 versus CNES/CLS).

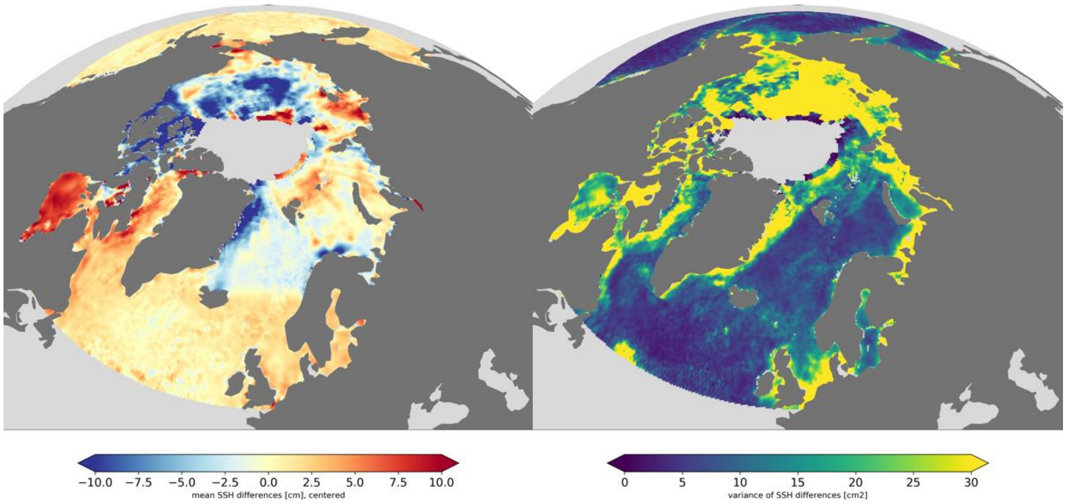

Figure 16, mean (left) and variance (right) of SSH differences between the Arctic Ocean dataset and DUACS global grids

We also express the variance of SSH differences as a fraction of the total SLA variance in DUACS grids (who are likely the best estimate of true SLA variance). The resulting map is shown on Figure 17. This indicates that despite the low levels of variance of SSH differences, the differences can be as energetic as the signal itself in some low variability areas of the ocean… Regarding concerns about continuity between the global and Arctic products, this will have to be investigated.

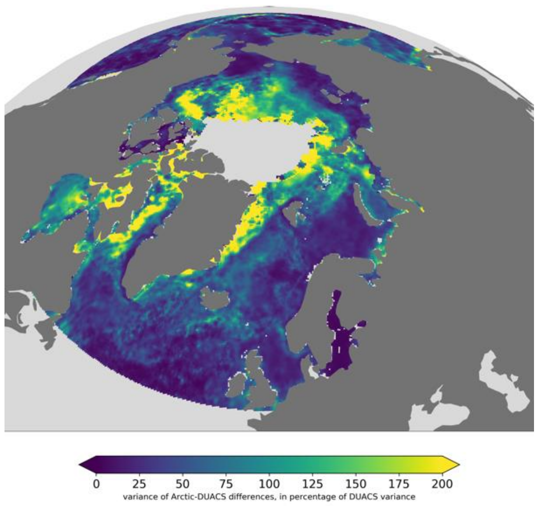

Figure 17, variance of SSH differences as a percentage of DUACS variance

7.4. Comparisons to tide gauges

Tide gauges provide in-situ measurements of sea-surface height and are avery valuable data source for the validation of out altimetric product. Here we present some examples of comparisons between the multi-mission product and tide gauges in the Arctic Ocean. Overall these comparisons suggest that there is some skill in the altimetry dataset, even at relatively high temporal frequencies (periods around ten days), where high frequency tide gauge measurements are available.
In the interior of the basin, a recent update of CLS tide gauge database allows to draw comparisons with PSMSL tide gauges at a monthly resolution again showing some level of agreement between altimetry and in-situ. When comparing to monthly tide gauges time series, the altimeter record was smoothed using a moving window filter.

Two tide gauges in the Barents and Baltic Seas are shown on Figure 18. Both stations show a good agreement between in-situ and altimetry measurements. For the Barents Sea, where high rate data is available, it is pretty clear that even high frequency signals are consistent.

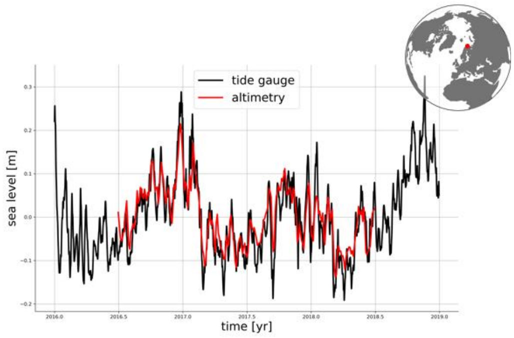

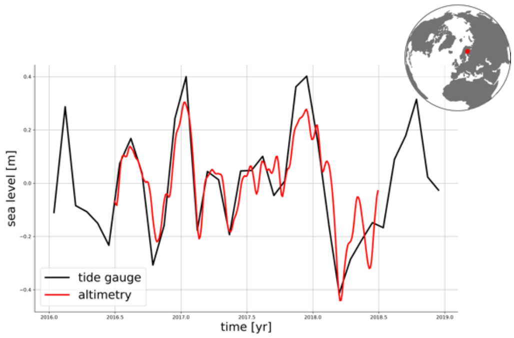

Figure 18, tide gauges versus altimetry comparisons in the Barents Sea and Baltic Sea

Along the Russian Arctic coasts, stations are less abundant and only available at a monthly resolution. In the East Siberian Sea where sea-ice is formed at the beginning of winter, two stations have near complete time coverage for both altimetry and tide gauges and exhibit consistent patterns (Figure 19).

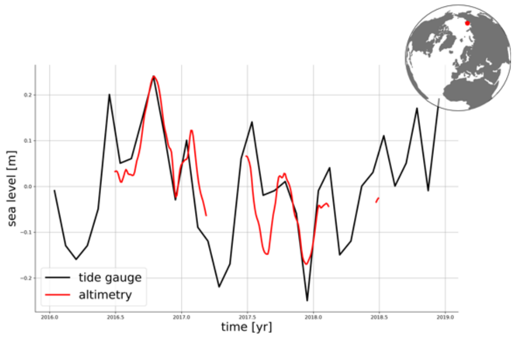

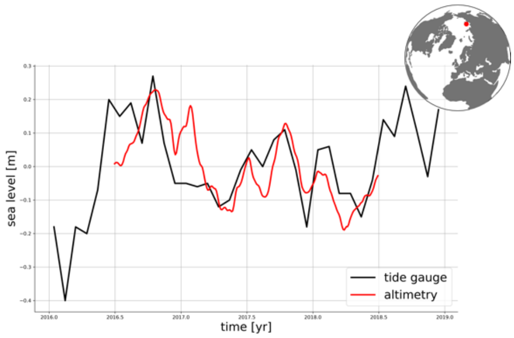

Figure 19, comparisons between tide gauges and altimetry in the East Siberian Sea

On the American and Canadian sides of the Arctic, one station in the Beaufort Sea and one up Baffin Bay near the Canadian Arctic Archipelago show a good agreement

FORM-NT-GB-7-1

with our altimetry dataset (Figure 20). Both these areas are covered by sea-ice during the winter.

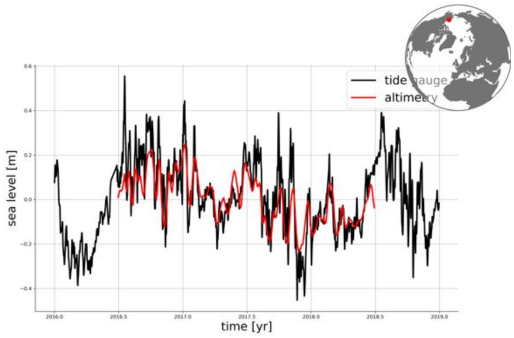

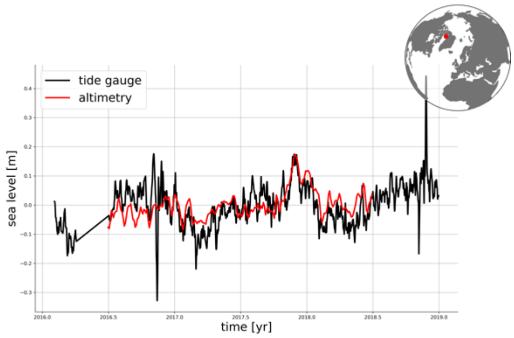

Figure 20, comparisons between altimetry and tide gauges in the American and Canadian Arctic

Even in Hudson Bay, and despite a large gap in the tide gauge measurements, high and low frequency variations in both records appear to match (Figure 21).

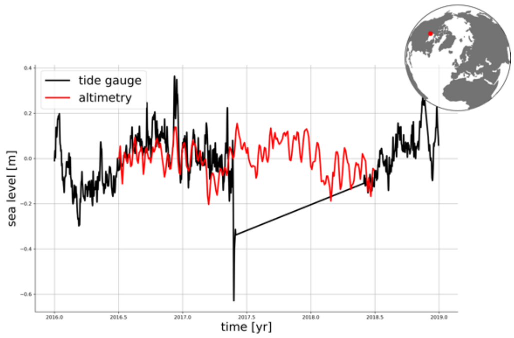

Figure 21, comparisons between altimetry and tide gauge in Hudson Bay

8. Conclusions

We were able to generate multi-mission maps of sea level anomaly for the Arctic Ocean, based on the along-track data generated as part of Task 1.1 of the CNES Alti Doppler Glaciologie contract.
Along-track data were extracted and pre-processed to compute residuals, which are used as the input of the mapping method. After updating a priori variables we use the classical DUACS optimal interpolation scheme to estimate SLA fields.
The SLA fields are estimated on a 25 km grid, every three days for all latitudes greater than 50°N. While this is an improvement over the mono-mission product resolution (75 km, monthly), it is not the effective resolution of the field, which is lower. The full process is documented in the present report.

We performed a qualitative performance assessment of the product. Results suggest that the performance of the product is good, especially with respect to tide gauges available in the basin. In particular, comparisons to high rate in-situ data show that signals with periods of about 10 to 15 days are consistently observed, even in seasonally ice-covered regions. Of course these comparisons do not provide information about the spatial resolution of the product.

Other metrics however highlight the limitations of the product:

- The mean sea surface model (DTU15) used is certainly inaccurate in at least two places: at 66°N in the Atlantic Ocean and in the CryoSat-2 SARIn box. That will induce wrong circulation when converting to ADT.
- Continuity with the global DUACS product is not achieved, and large differences of the order of magnitude of the signal are observed in low variability areas of the ocean,

Directions for improving the product quality are also identified, which are independent of the ones cited in DR7:

- Re-estimating the signal covariance scales, this could be done from this dataset, in an iterative way, from the along-track data themselves or from a suitable model,
- Adapting the empirical orbit error reduction algorithm for regional analysis,

List of acronyms

TBC	To be confirmed
TBD	To be defined
AD	Applicable Document
RD	Reference Document